Research Article Vol. 57, No. 22 / 1 August 2018 / Applied Optics E89

Numerical investigation of a feed-forward linewidth reduction scheme using a mode-locked laser model of reduced complexity

Sean O'Duill,[1,*] M. Omar Sahni,[2] Stéphane Trebaol,[2] Pascal Landais,[1] L. Bramerie,[2] Stuart G. Murdoch,[3] Pascal Besnard,[2] and Liam P. Barry[1]

[1]Radio and Optics Research Laboratory, School of Electronic Engineering, Dublin City University, Glasnevin, Dublin 9, Ireland
[2]Univ. Rennes, CNRS, Institut FOTON—UMR 6082, F-22305 Lannion, France
[3]The Dodd-Walls Centre for Photonic and Quantum Technologies, Department of Physics, The University of Auckland, Auckland 1142, New Zealand
*Corresponding author: sean.oduill@dcu.ie

Received 16 February 2018; revised 24 May 2018; accepted 24 May 2018; posted 29 May 2018 (Doc. ID 320808); published 29 June 2018

We provide numerical verification of a feed-forward, heterodyne-based phase noise reduction scheme using single-sideband modulation that obviates the need for optical filtering at the output. The main benefit of a feed-forward heterodyne linewidth reduction scheme is the simultaneous reduction of the linewidth of all modes of a mode-locked laser (MLL) to that of a narrow-linewidth single-wavelength laser. At the heart of our simulator is an MLL model of reduced complexity. Importantly, the main issue being treated is the jitter of MLLs and we show how to create numerical waveforms that mimic the random-walk nature of timing jitter of pulses from MLLs. Thus, the model does not need to solve stochastic differential equations that describe the MLL dynamics, and the model calculates self-consistently the line-broadening of the modes of the MLL and shows good agreement with both the optical linewidth and jitter. The linewidth broadening of the MLL modes are calculated after the phase noise reduction scheme and we confirm that the phase noise contribution from the timing jitter still remains. Finally, we use the MLL model and phase noise reduction simulator within an optical communications system simulator and show that the phase noise reduction technique could enable MLLs as optical carriers for higher-order modulation formats, such as 16-state and 64-state quadrature amplitude modulation.

OCIS codes: (140.0140) Lasers and laser optics; (140.5960) Semiconductor lasers; (140.4050) Mode-locked lasers; (270.2500) Fluctuations, relaxations, and noise; (060.0060) Fiber optics and optical communications.

https://doi.org/10.1364/AO.57.000E89

1. INTRODUCTION

Mode-locked lasers (MLLs) are multi-longitudinal mode lasers with a fixed frequency difference between each lasing mode and with each mode ideally possessing the same phase noise. The resulting phase relationship between the modes means that a periodic temporal output emanates from these type of lasers ([1,2], including references therein). The locking of modes can be accomplished in a number of ways: (i) actively by applying an external sinusoidal or periodic modulation at a frequency equal to the laser free spectral range (FSR) [1,2]; (ii) passively whereby a saturable absorber or nonlinear element is placed/integrated into the cavity that can open a short net-gain window allowing for pulsations to form [1–3]; (iii) hybrid mode locking, which is a combination of both active and passive mode locking [4,5]; and finally, (iv) some single-section multi-mode Fabry–Perot lasers are known to mode-lock without help of either external modulation or saturable absorption [6–8]. In those cases, the mode-locking mechanism is possible due to a phase transfer that synchronizes all the modes. It is brought by an internal beating (i.e., modulation) between the modes that in turn generates sidebands spaced by the FSR about each mode and hence these sidebands couple close to adjacent modes. The coupled photons in each sideband have the same phase relationship with those of the modes and have more power than the spontaneous emission; therefore, the phase synchronizing mechanism in (iv) is likely to be a four-wave mixing process [6,9]. Single-section Fabry–Perot MLLs typically possess of the order of 10 equipower modes within a few terahertz bandwidth [7,8], and are attracting broad interest across numerous applications, the main applications being: terahertz signal generation [10] and as multi-carrier sources within compact transceivers for short-range

communications due to their low form factor, low power consumption, and large FSR in the tens of gigahertz range [11,12]. This large FSR allows for easy optical bandpass filtering of the individual modes so that each mode can be modulated independently using a variety of exotic modulation formats [11–15] with symbol signaling rates approaching 100 GBaud. Unfortunately, the large linewidth of the MLL, typically of the order of tens of megahertz, is too broad to be able to transmit data encoded using the phases of the MLL modes. To this end, an optical heterodyne-based phase noise reduction scheme [16,17] was devised to reduce the linewidth of the modes to that of the local oscillator (LO) laser used in the scheme; impressive reductions in intrinsic linewidth to a few tens of hertz have been demonstrated [18] with the phase noise limited by the high-quality LO used [16–18]. The phase noise reduction scheme allowed 30 comb lines from a single-section MLL to be used for the coherent transmission of data encoded with quadrature phase shift keying on each comb line [19,20]. The phase noise reduction technique requires a beat signal using a high-quality single-wavelength laser source as an LO. This beat signal is fed forward to modulate the light from the MLL thus creating a pair of sidebands about each mode. The lower sidebands (the lower-frequency sideband about each mode), have the phase noise of the LO. Optical filtering is required to suppress all of the undesired sidebands from the output, leaving only the MLL with reduced phase noise.

In this paper, we verify the feed-forward phase noise reduction scheme through a complete numerical approach. We modify the heterodyne phase noise reduction scheme by using single-sideband optical modulation thus the lower-frequency modulation sidebands with the reduced phase noise are just kept at the output and no optical filtering would be required [21]. In order to validate the phase noise reduction scheme, we develop a simplistic numerical MLL model based on a recirculating pulse in a resonator that includes pulse round-trip jitter and phase noise, the schematic of which is shown in Fig. 1. For modeling timing jitter in MLLs, generating a numerical random walk is needed and has been successfully shown to capture the timing jitter spectrum of MLLs [22]; however, difficulties arise when trying to impose the jitter onto a numerical representation of the MLL pulse train because of the finite signal sampling time. We overcome these issues by implementing a style of Schmitt trigger that converts the numerically generated random-walk jitter into a form that can be implemented on a pulse train.

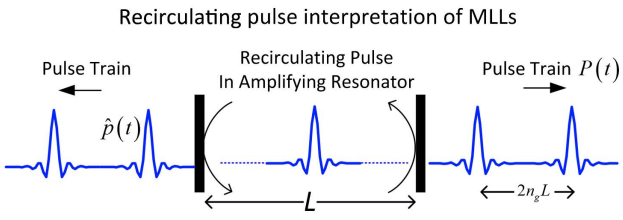

Fig. 1. Schematic of a recirculating pulse within a resonator. Mode locking in a laser has occurred when the output has periodicity of the resonator round-trip time. n_g is the group index, L is the length of the resonator. The temporal period of the pulse train is $2n_gL/c$, where c is the speed of light.

This approach allows us to create numerical waveforms that capture all of the phase noise characteristics of MLLs without resorting to solving complicated stochastic differential equations describing the MLL [3,5,19], and moreover allows us to calibrate the waveform in terms of the easily measurable MLL quantities, such as the FSR, optical linewidth, jitter (characterized as an equivalent RF linewidth), and spectral extent. These are the only specified parameters required as input to the MLL model. We show how to calibrate the temporal jitter of the MLL pulses in terms of the RF linewidth and we verify that relationship by calculating the FM-noise spectral density of each MLL mode and showing that the values are as expected from the theory for the line broadening of MLL modes (that the timing jitter induces a mode-index-dependent linewidth that follows a quadratic dependence on the mode index number). We verify that the residual phase noise remaining after the MLL has undergone a phase noise reduction technique is that phase noise contribution arising from the temporal jitter of the pulses. We finally show how the phase noise of the MLL can be reduced to levels that allow for 16- and 64-quadrature amplitude modulation (QAM) signals to be carried by MLLs, and we recommend simulation parameters in order to improve the accuracy of the system simulations.

2. MODE-LOCKED LASER MODEL

The spectral properties of optical frequency combs can be replicated numerically simply by constructing a temporal pulse train and including both phase noise and appropriate timing jitter for each individual pulse. We have done this previously for understanding the peculiarities of the spectra of gain-switched lasers in [23]. There is one crucial aspect in which pulsations from MLLs differ from the pulsations of gain-switched lasers and that is for MLLs the timing position of the current pulse depends on the accumulated (random-walk or Brownian motion) timing jitter from preceding pulses whereas for gain switched lasers the timing jitter of the current pulse has no memory of the timing jitter of the preceding pulses. While in principle the modes of the MLL possess the same phase noise, the additional phase noise seen by each mode arising from the random-walk nature of the MLL timing jitter results in the modes of the MLL experiencing a quadratic increase of the linewidth [2,24–26].

To begin we start by creating a sinc-style pulse because of the flat, rectangular spectrum associated with sinc pulses. Thus, we let

$$\hat{p}(t) = \mathrm{sinc}(t/T_s) W_{T_p}, \tag{1}$$

with $\mathrm{sinc}(x) = (\pi x)^{-1} \sin(\pi x)$ and T_s defines the temporal profile of the sinc pulses, T_p is the time period of the pulsation and is related to the mode spacing or FSR by $\Delta\upsilon_{\mathrm{FSR}} = T_p^{-1}$. In order to create narrow pulses and hence a frequency comb with a wide bandwidth we require the condition that $T_p > T_s$. W_{T_p} is a window function that confines each sinc pulse to a temporal slot equal the pulse repetition period, and the windowing function narrows the pulse to further broaden the spectral extent of the pulses. The effect of the window W_{T_p} is to also adjust the relative amplitude of the modes in the MLL spectrum so that a flat optical frequency comb can be generated as well as

providing a sharp cutoff in the spectral extent of the overall comb. Choosing a window W_{T_p} for our purposes is a matter of taste and we used a Kaiser–Bessel window with parameter 10 [27]. One may use differing pulse shapes and windows to replicate the spectrum of any desired optical frequency comb/MLL. A representation of the pulse shape $\hat{p}(t)$ adopted by this paper was used in constructing Fig. 1. The entire pulse train $P(t)$, with pulses repeating with the same cavity round-trip time as the MLL, can be constructed by convolving $\hat{p}(t)$ with a train of delta functions each separated by T_p, plus the accumulated timing jitter apart. Finally, the phase noise is included by multiplying the entire pulse train by a phase noise term that accounts for the common optical phase noise experienced by all of the MLL modes:

$$P(t) = \left[\sum_n \delta(t - nT_p - \Delta\tau_{j,n}) \otimes \hat{p}(t)\right] \exp[j\phi(t)]. \quad (2)$$

Or equivalently writing Eq. (2) as the sum of the individual modes

$$P(t) = \sum_m P_m \exp\left\{j\left(2\pi m \Delta\upsilon_{\mathrm{FSR}} t + 2\pi m \frac{\Delta\tau_j(t)}{T_p}\right)\right\} \exp(j\phi), \quad (3)$$

where n is the temporal index of the nth pulse, $\Delta\tau_{j,n}$ is the timing jitter offset associated with the nth pulse, and ϕ is the common phase noise of the MLL that is experienced by all of the modes. P_m is the field of the mth indexed mode and related to the Fourier series coefficients of $\hat{p}(t)$. The (optical) spectrum of such a field will be comprised of distinct laser modes as outlined in Eq. (3) with m being the modal index number. The phase noise of each mode has two contributions: ϕ, which is the phase noise common to all of the modes, and a different additional phase noise component for each mode arising from the jitter $2\pi m \Delta\tau_j / T_p$. It is well known that jitter causes a quadratic increase in the linewidth of the modes with respect to the mode index number [2,26].

In our simulation framework, the zero index coincides with the central line of the MLL when taking a fast Fourier transform of Eq. (2). If we label the mode index as "m" with sufficient mode indices $[-m\ -(m-1)\ \ldots\ -1\ 0\ 1\ \ldots\ (m-1)\ m]$ to extend over the entire range of the MLL spectrum, then the combined phase noise of the mth mode can be written as [26]

$$\phi_m = \phi + 2\pi m \frac{\Delta\tau_j}{T_p}, \quad (4)$$

where $\Delta\tau_j$ is the jitter experienced by the pulse train. Therefore, each pair of adjacent modes experience a relative phase difference of $2\pi\Delta\tau_j / T_p$. In order to fully quantify the phase noise in our model, we only need to specify the phase noise ϕ and the timing jitter $\Delta\tau_j$ and this will produce a numerical quantity that mimics the spectral properties of MLLs. Both ϕ and $\Delta\tau_j$ are easily related to measurable quantities, such as optical linewidth and the RF linewidth. The RF linewidth is found by filtering out two adjacent modes from the MLL spectrum and beating them on a photodiode with sufficient bandwidth to capture the beat component, and then using an electrical spectrum analyzer to measure the linewidth. The RF linewidth B_{RF} is independent of the pair of modes filtered from the MLL [10], i.e., $\phi_m - \phi_{m-1} = 2\pi\Delta\tau_j T_p^{-1}$. The optical linewidth for each mode can be found using the standard techniques, such as the delayed self-heterodyne method. The total optical linewidth of the mth mode is given by [26]

$$B_O^{(m)} = B_O + m^2 B_{\mathrm{RF}}. \quad (5)$$

Even though we make no reference to the spontaneous emission in this work, spontaneous emission is responsible for both the optical linewidth and timing jitter in the MLL [28]. Spontaneous emission is a random process with Poissonian statistics; we assume that much more than one spontaneous emission event occurs within each sampling time and via the central limit theorem we can use Gaussian statistics to generate all of our random sources. The random-walk quantities, ϕ and $\Delta\tau_j$, are generated by calculating a cumulative sum of appropriately scaled random values obtained from a Gaussian distribution. We generate the phase noise ϕ as [29]

$$\phi(l) = \sigma_\phi \sum_{k=0}^{l} \varphi(k), \quad (6)$$

with

$$\sigma_\phi = \sqrt{2\pi B_O t_s}. \quad (7)$$

In Eq. (6) $\varphi(k)$ describes the phase noise increment of the MLL field over the kth sampling period. $\varphi(k)$ are random samples taken from a unity-variance, zero-mean Gaussian distribution with a sample point taken for every sampling point of the MLL field. The action of Eq. (6) computes a cumulative sum of the incremental phase noise quantity $\varphi(k)$, and therefore, $\phi(l)$, which is phase noise at the lth sampling instance of the MLL field, is the scaled sum of all previous increments for $\varphi(k)$ with $0 \le k \le l$. The scaling in Eq. (7) calibrates the phase noise such that B_O is the linewidth [29]. The sampling period of the MLL field is t_s and throughout this paper we set $t_s = 1$ ps.

We now calibrate the timing jitter in terms of the RF linewidth. In Eq. (3) we note that the extra phase change of the $m = 1$ mode of the MLL due to the timing jitter is given as

$$\Delta\phi_j^{m=1} = 2\pi \frac{\Delta\tau_j}{T_p}. \quad (8)$$

The RF linewidth defines the equivalent phase noise that produces the same phase shift for the $m = 1$ mode as does the timing jitter. We use a similar random-walk generation technique in Eq. (6) and modify it to generate a random-walk waveform for the jitter. The jitter to phase noise conversion was performed in Eq. (8), whereby the equivalent phase shift involves dividing the jitter value by the pulse repetition period T_p and multiplying by 2π; in other words, a timing jitter event equal to the pulse repetition period induces a 2π phase shift for the $m = 1$ mode. Using the same principle as in Eq. (6), we need to calculate an equivalent standard deviation, denoted σ_j, of the incremental timing jitter acquired by the pulse during each round trip. The jitter is calculated on a pulse-by-pulse basis and therefore the time step t_s in Eq. (7) needs to be replaced by T_p and the RF linewidth B_{RF} replaces the optical linewidth. Therefore, replacing the left-hand side of Eq. (8) using a modified version of Eq. (7) yields an scaling the jitter for the phase shift of the $m = 1$ mode:

$$2\pi\frac{\sigma_j}{T_p} = \sqrt{2\pi B_{\mathrm{RF}} T_p}, \tag{9}$$

and σ_j is the standard deviation of the incremental jitter that updates on a pulse-per-pulse basis. Rearranging Eq. (8), we get

$$\sigma_j = \sqrt{\frac{B_{\mathrm{RF}} T_p^3}{2\pi}}. \tag{10}$$

It should be noted that this formula (10) could also be derived by considering the line shape of the RF beat tone and deriving the timing jitter using equivalency formulas as was done in [30], though here we are deriving the equation from first principles based on converting the jitter to a phase and scaling that phase to set a desired B_{RF}. Our results for the FM-noise spectral density (linewidth) of each mode will show that Eq. (10) is correct. Now we are in a position to compute appropriately calibrated pulse timing jitter for our MLL waveform. The timing jitter for the pulse train is computed as

$$\Delta\tau_{j,n} = \sigma_j \sum_{q=0}^{n} \Delta\tilde{\tau}_{j,q}, \tag{11}$$

where $\Delta\tilde{\tau}_{j,q}$ are random samples taken from a unity-variance, zero-mean Gaussian distribution, and there are as many samples for $\Delta\tau_{j,n}$ taken as there are pulses in the pulse train. The random waveforms for φ_k in Eq. (6) and $\Delta\tilde{\tau}_j$ in Eq. (11) must be taken from two separate, uncorrelated, unity-variance Gaussian distributions.

Even though we can generate a calibrated jitter waveform, unfortunately the finite numerical sampling period (picosecond time scale) limits our ability to shift the pulses in accordance with the timing jitter, which is of the femtosecond time scale. Therefore, we can only shift the pulses once the accumulated jitter exceeds an integral number of the signal sampling time. This problem does not arise when implementing the phase noise because the phase noise increment at each time step can be fully captured by the computer's ability to represent numbers using the double-precision floating point format. We have a lot of experience in generating laser phase noise [23,31–33], though generating pulse timing jitter represents a new challenge due to the granularity of the allowable jitter increments and decrements. The experience gained by granulizing the jitter to be integral numbers of the sampling time informs us that simply thresholding the jitter increments (decrements) to the nearest value of the true accumulated jitter can result in multiple jitter instances that exacerbate the FM noise of the modes. We find that, by implementing a style of Schmitt trigger that forbids successive jitter increments (decrements) until the accumulated jitter has increased (decreased) by at least the signal sampling time t_s from where the previous timing jitter increment (decrement) occurred, does not introduce malicious artifacts into the MLL waveform. An example of the numerical generated jitter waveform with the implemented jitter transitions is shown in Fig. 2.

We now summarize the generation process of the numerical MLL waveform. The pulse train in Eq. (2) is constructed as follows: given the sampling time t_s, the number of samples per pulse is $(t_s \Delta\upsilon_{\mathrm{FSR}})^{-1}$ and a sinc pulse is constructed with this number of samples. In order to perform the convolution operation in Eq. (2), we need to create a numeric array comprising of a train of appropriately spaced delta functions. Ideally in the absence of jitter, each delta function would be spaced by the number of samples per pulse; in the presence of jitter, the delta function of the nth pulse must be shifted from the expected instance (nT_P) by the timing jitter $\Delta\tau_{j,n}$ [Eq. (11)]. An entire array whose length equals the number of pulses multiplied by the samples per pulse, is initialized with zeros. In this array, a "one" is inserted [corresponding to the δ-function in Eq. (2)] at integral multiples of the samples per pulse, though the positioning of the "one" is offset from the desired array index by the accumulated jitter in Eq. (11). Then finally the total field is multiplied by the phase noise term $\exp(i\phi)$, with ϕ calculated using Eq. (6). The simulation parameters are listed in Table 1. The FSR of $27.\dot{7}$ GHz is chosen such that T_p is 36 ps and importantly an integer multiple of the sampling period, which is 1 ps. The values of the optical and RF linewidths are chosen to match values measured from quantum-dash-based passively mode-locked laser diodes [24], though they can be adjusted to match any desired value. The number of pulses generated is 20,000.

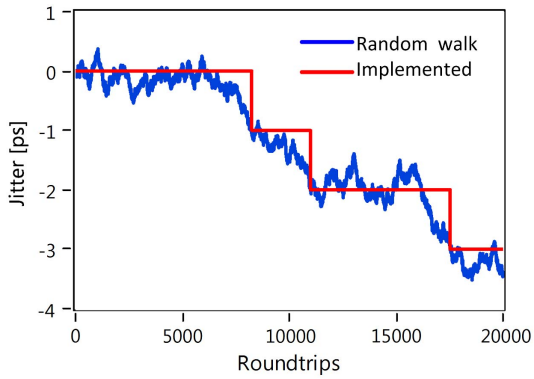

Fig. 2. Numerically generated random-walk jitter in blue as a function of the number of cavity round trips for an RF linewidth of 20 kHz. The red curve shows the implementable timing jitter in the MLL simulator.

Many of the results in this paper rely on observing line broadening of the MLL modes; for clarity we show the quality of the MLL spectrum in the absence of both jitter and phase noise. We begin by omitting the jitter and phase noise and generating a pulse train using Eq. (2). From this pulse train the spectrum can be calculated with the aid of a fast Fourier transform. The spectrum of the ideal MLL is plotted in Fig. 3. With a 1 ps sampling period and 720,000 samples the spectral resolution of 1.39 MHz. The ideal pulse train clearly shows

Table 1. MLL Simulation Parameters

Symbol	Quantity	Value
B_O	Optical linewidth	10 MHz
B_{RF}	RF linewidth	20 kHz
t_s	Sampling period	1 ps
$\Delta\upsilon_{\mathrm{FSR}}$	MLL repetition rate	27.7777 GHz
T_s	Time parameter of sinc	$0.02 \times T_p$

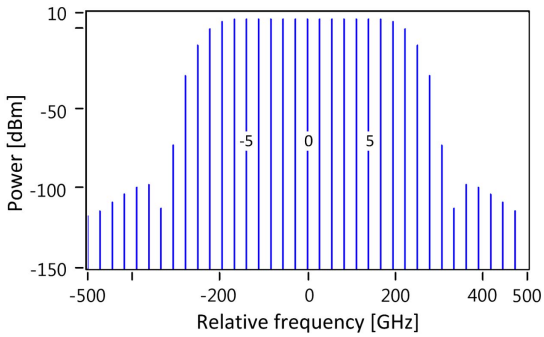

Fig. 3. MLL spectrum using the pulse described in the text with an FSR of 28 GHz. The spectrum was obtained without adding any noise source terms and serves as a reference for all other spectra shown in this paper. The mode index m of the −5th, 0th, and 5th modes are indicated.

delta-style lines for each of the modes. When we add in the random terms, the modes will exhibit a Lorentzian line broadening. We initially add in the timing jitter related to the RF linewidth of 20 kHz and keep the optical linewidth at zero. The spectrum is shown in Fig. 4(a); notice how there is no line broadening whatsoever of the central mode ($m = 0$), whereas there is a visible increase in the line broadening commensurate with the square of the mode number and this will be explored in more detail later. When the underlying optical linewidth of 10 MHz is then added, each of the lines undergoes an additional 10 MHz line broadening, as presented in Figs. 4(b) and 4(c).

Even though the line broadening of the modes is visible in Fig. 4, there is no quantifiable result that would imply that the MLL model is correct. Therefore, we filter out each individual mode and calculate the FM-noise spectral density [34]. We only use a Gaussian-shaped optical bandpass filter with a 3 dB bandwidth of 7 GHz throughout this paper. The calculated FM-noise spectral density curves of the MLL with optical linewidth of 10 MHz and 20 kHz RF linewidth are shown in Fig. 5. Multiplying the value of the one-sided FM-noise spectral density by π gives an estimate for the commonly understood Lorentzian linewidth and this is done throughout so that we can compare the curves with the linewidth values input to the simulator. The aggressive optical filtering causes the value of the FM noise to reduce after 1 GHz and we ignore values beyond 1 GHz. The average FM-noise curve is just above 10 MHz with a slight increase in the FM noise with increasing mode index number. The increase in linewidth due to the timing jitter is 2 orders of magnitude lower than the 10 MHz optical linewidth and will be explored in more detail shortly. The calculated FM-noise spectral density of 10 MHz agrees with the value of 10 MHz set by simulator in Table 1. Even though it is possible to extract the component due to the jitter in Fig. 5, to make a more visually convincing case we generate an MLL field by setting the optical linewidth term $\phi = 0$ in Eq. (2). We then filter each mode and plot the FM-noise spectral density in Fig. 6. Now we can clearly see the impact of the temporal jitter on the linewidth of the modes. For mode index "0," this has zero FM-noise spectral density, while the other modes show a quadratic increase in the values in the FM-noise spectral density

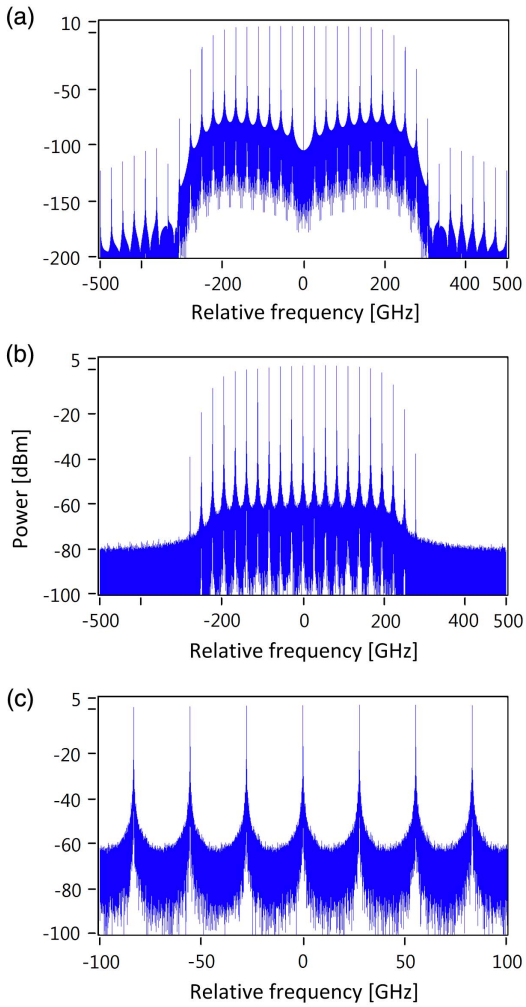

Fig. 4. Generated MLL spectra when adding the jitter and optical phase noise terms. (a) MLL spectrum when only considering pulse jitter. The RF linewidth is 20 kHz. (b) MLL spectrum considering both jitter and phase noise. The optical line broadening is 10 MHz. (c) Zoom of portion of (b) over a 200 GHz span to show the line broadening of the MLL modes. The spectral resolution is 1.39 MHz.

as expected from Eq. (5). It should be noted, however, that the value for the FM noise of the mode with index "1" should equate to the RF linewidth. The RF linewidth was set to 20 kHz, though the estimated value is ∼16 kHz, which is just short of 20 kHz. Experience running the simulator informs us that there is a spread in the FM-noise values that average about 20 kHz. The trend with MLL mode index number clearly shows the expected quadratic increase in the FM-noise spectral density. Note that these values for FM-noise spectral density will be useful in verifying the operation of the phase noise reduction scheme in the following section.

3. SINGLE-SIDEBAND HETERODYNE-BASED PHASE NOISE REDUCTION SCHEME

In this section we present numerical results to validate the feed-forward phase noise reduction scheme and to verify the

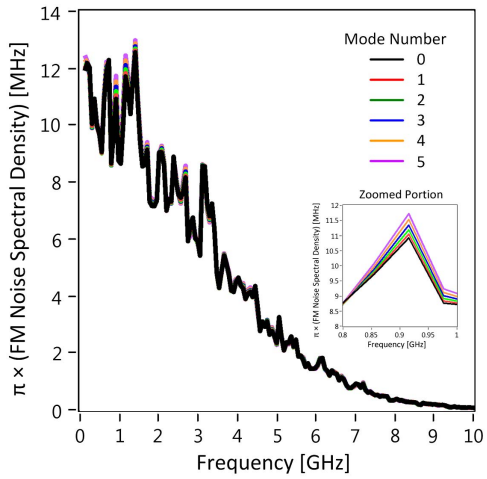

Fig. 5. FM-noise spectral density calculation of modes filtered from the generated MLL field with RF linewidth (jitter) of 20 kHz and optical linewidth of 10 MHz. At low frequencies, below 1 GHz, the FM-noise spectral density averages at 10 MHz as expected. Note the slight increase in FM-noise spectral density with respect to increasing mode index number. The zoomed portion in the inset shows the increase in FM noise with mode index number.

linewidth properties of the MLL after undergoing phase noise reduction. The inclusion including single-sideband optical modulation to the heterodyne concept of the phase noise reduction technique results in only the phase noise reduced components of the MLL remaining after optical modulation, thus no optical filtering is required [21]. The operation schematic is shown in Fig. 7. At point "A" the light from the MLL emerges and is split along two paths. Ninety percent of the light will be modulated to undergo phase noise reduction; the other 10% of the power is used to generate the modulating signal that will

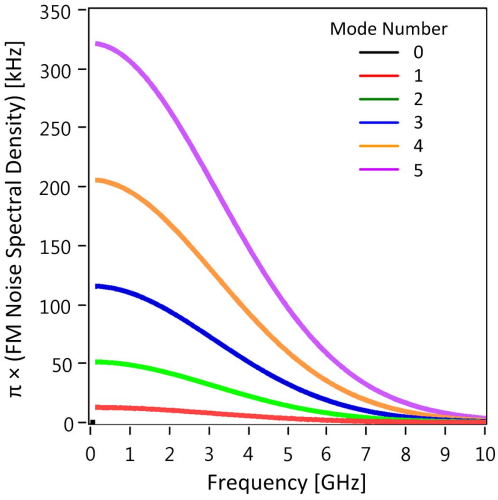

Fig. 6. FM-noise spectral density calculation of the MLL field when only considering jitter. The low-frequency portion of the FM-noise spectral density below 1 GHz gives an indication of the linewidth of the modes. The RF linewidth was 20 kHz and a clear quadratic increase in linewidth of the modes with respect to mode number index is evident.

impose phase noise reduction on the MLL. The modulating signal is created by heterodyning one comb line from the MLL with the light output from a single-wavelength laser, which we also term as local oscillator (or LO). The phase noise reduction scheme requires a single-wavelength LO laser at point "B" with superior phase noise properties to those of the MLL and the central wavelength of the LO laser must be spectrally close to the central comb line from the MLL. Numerically the field for the LO is given by

$$E_{\mathrm{LO}}(t) = A_{\mathrm{LO}}\ \exp(j[2\pi\Delta f_D t + \phi_{\mathrm{LO}}]), \tag{12}$$

where A_{LO} is the amplitude of the LO field, and set equal to 1. Δf_D is the detuning between the LO laser and the nearest mode in the MLL, and ϕ_{LO} is the phase noise term of the LO, which is uncorrelated to that of the MLL. The heterodyned beat signal is generated by combining the light from the MLL and LO laser and creating an electronic heterodyned beat signal at the balanced detector. The heterodyned beat signal will subsequently be used to modulate the original MLL field. The electrical output from the balanced photodetector is low-pass filtered and the electrical voltage at point "C" is proportional to

$$V_C \propto |E_{LO}||E_{MLL,0}|\ \cos(2\pi\Delta f_D t - \phi + \phi_{LO}), \tag{13}$$

where E_{LO} is the optical field of the LO laser, $E_{\mathrm{MLL},0}$ describes the optical field of the spectrally closest mode of the MLL to the LO; we take the nearest MLL mode to be "0" mode. Δf_D is the detuning between the LO laser and the nearest mode in the MLL. In our system, the phase noise of the "0th" mode of the MLL is ϕ as defined in the previous section. Beat components from the other modes in the MLL will also contribute to the output from the balanced photodiodes, though these are suppressed by the limited bandwidth of the photodiodes themselves and we use a low-pass filter to ensure that only the specific beat term described in Eq. (13) dominates. An RF amplifier is used to supply sufficient drive voltage to the electro-optic optical I-Q modulator. In order to generate a single-sideband signal we need to split the RF modulating signal using an RF power splitter (also known as a 6 dB splitter) into two separate arms. To implement the single-sideband modulation for a pure sine wave, the sine wave that drives the "Q"-arm of the I-Q modulator must be delayed by one quarter of the period relative to the sine wave that drives the "I"-arm of the I-Q modulator. In our simulation we apply a relative delay of $(4\Delta f_D)^{-1}$ to the modulating voltage that is applied to the "Q"-arm. This delay is equivalent to a $\pi/2$ phase shift for the sine wave of frequency Δf_D and needed to ensure single-sideband output from the I-Q modulator [35]. Both of the Mach–Zehnder arms are biased at their null points hence the π phase shifts in both of the individual Mach–Zehnder modulators in the optical I-Q modulator to suppresses the field of the original MLL in the output.

Mathematically the field output at point "D" can be described as

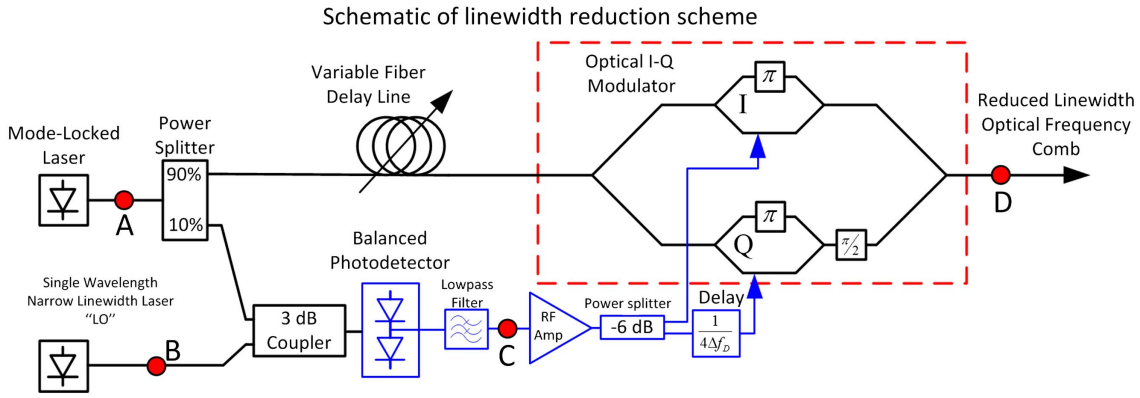

Fig. 7. Schematic of the single-sideband phase noise reduction scheme is shown. The idea is to reduce the phase noise of the MLL to be that of the narrow-linewidth single wavelength LO laser. A voltage containing the phase difference information between the LO and MLL is generated at the balanced photodetector and that signal is then applied to the MLL field in order to modulate each MLL mode in such a fashion that each mode has the phase noise properties of the narrow-linewidth LO. The optical I-Q modulator and RF delay by one quarter period of the MLL-LO detuning results in single-sideband modulation of the MLL modes.

$$E_{\text{out}}(t) = \frac{\sqrt{0.9}E_{\text{MLL}}(t)}{2} \times \left\{ \left[\exp\left(\frac{K\pi V_C(t)}{V_\pi} \right) - 1 \right] + j\left[\exp\left(\frac{K\pi V_C(t - (4\Delta f_D)^{-1})}{V_\pi} \right) - 1 \right] \right\}, \quad (14)$$

where $E_{\text{MLL}}(t)$ is generated using Eq. (2) above, $V_C(t)$ is generated by low-pass filtering $\sqrt{0.1}E^*_{\text{MLL}}(t)E_{\text{LO}}(t)$, V_π is the voltage required to induce a phase shift of value π in the modulated optical field, and K is a scaling factor that increases the applied voltage to be commensurate with V_π. A fiber delay line ensures synchronization between the applied voltage modulation to the MLL field, and the MLL field that created the applied voltage through beating with the LO. The LO field could be generated in a manner similar to that described for the optical linewidth in Eq. (6) and using 10 kHz as the value of the optical linewidth of the LO. Though instead we use our laser phase noise generator to create the field for the LO laser [31]; this includes the resonance-enhanced phase noise arising from the carrier-photon interaction in semiconductor lasers [36]. The laser parameters of the LO are as follows: linewidth of 10 kHz, alpha-factor = 3, relaxation oscillation at 8 GHz, and a damping rate of 1×10^9 s^{-1}. All of these parameters are measurable quantities for semiconductor lasers and their respective values can be directly included when implementing the model for resonance-enhanced phase noise in [31]. For the purposes of this paper, the linewidth is considered to be the most important quantity, and we set the LO linewidth to a low value of 10 kHz to conclusively show the linewidth narrowing of the MLL. For completeness, we choose reasonable values for the relaxation frequency, damping rate, and alpha-factor. The linewidth of the LO laser is 10 kHz, which is much smaller than that of the MLL which is 10 MHz in this case. The spectrum of the LO laser is shown in Fig. 8, note the satellite peaks arising from the resonance-enhanced phase noise [31,36].

Now we are in a position to generate the field for the phase noise reduced MLL using Eq. (14). First we generate the field for the MLL $E_{\text{MLL}}(t)$ using Eq. (2), the LO field $E_{\text{LO}}(t)$ using

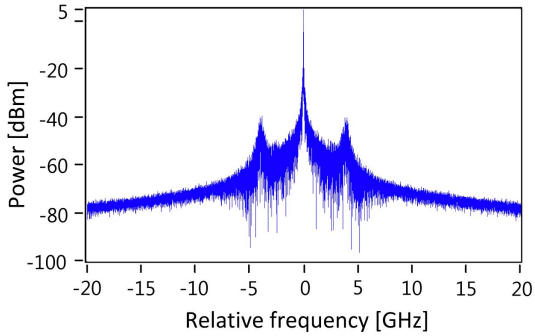

Fig. 8. Power spectrum of the narrow-linewidth LO laser. Its linewidth is 10 kHz though the carrier-photon resonance in the laser is included in determining the phase noise of the LO. The spectral resolution is 1.39 MHz.

[31] and Eq. (12), and the beat voltage $V_C(t)$ using Eq. (13). The phase noise reduced MLL field is shifted by Δf_D relative to the original MLL field. In this example, Δf_D is taken to be 5 GHz. The spectrum of the phase noise reduced MLL is shown in Fig. 9. The only components that remain in that spectrum are the lower-frequency sidebands with the spectral components possessing the phase noise of the LO. For clarity, we zoom in on individual comb lines for the "0" indexed mode and the fifth indexed mode, with the original MLL field superimposed for comparison in Fig. 10. Note the 5 GHz frequency shift between the MLL and phase noise reduced MLL; there is also an obvious reduction in the line broadening of the phase noise reduced MLL field compared to the original MLL field. Though looking at the line broadening of the field of the fifth indexed mode, the line broadening of the fifth indexed mode is greater than that of the zeroth indexed mode, because the phase noise reduction technique cannot compensate for the phase noise arising from the jitter in the MLLs. To formally quantify this broadening, we calculate the FM-noise spectral density of each of the modes after the phase noise reduction technique.

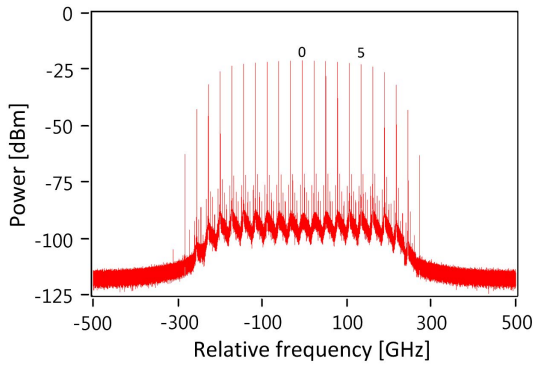

Fig. 9. Full spectrum of the MLL after the single-sideband feed-forward phase noise reduction scheme. Note that only the lower-frequency sidebands, the sidebands that possess the reduced phase noise remain in the spectrum. The original MLL and upper-frequency sidebands are suppressed by the modulation technique and no extra optical filtering is required to obtain this spectrum. Detailed quantification of the spectral quality is given in subsequent figures.

The results are shown in Fig. 11. The FM-noise spectral density of the phase noise reduced MLL shows that at low frequencies the FM-noise spectral density of the modes reduces to that of the MLL when only jitter is considered (see Fig. 6), with an additional 10 kHz linewidth from the LO laser. The increase in the FM-noise spectral density with increasing frequency arises from a number of causes: (i) low-pass filtering the high-frequency components of the beating between the MLL and LO laser after the heterodyning process means that the higher-frequency phase noise will not be completely cancelled; (ii) spectral leakage from the main MLL modes that have not been completely suppressed by the optical modulation when creating the reduced-linewidth MLL field. Beyond 1 GHz the FM noise decreases because each specific mode has been filtered out using a Gaussian-shaped optical bandpass filter with 7 GHz bandwidth.

An interesting result happens when the phase noise reduction technique is applied to an actively mode-locked laser. In this case the MLL is modulated by a high-quality RF source with narrow RF linewidth of a few hertz, thus effectively reducing the timing jitter to zero. The phase noise reduction simulations were performed again except this time, the RF linewidth for the MLL was set to 0 Hz with the optical linewidth of the MLL set to 10 MHz. The FM-noise spectral density results are represented by the black open squares in Fig. 11. Note that the squares overlap with the values for the "0th" mode for the case of the MLL with jitter because each mode in the actively mode-locked MLL has the exact same phase noise, and hence reduces to the same values.

The effectiveness of the phase noise reduction scheme can be displayed on a logarithmically scaled plot depicting the linewidth of the MLL before and after phase noise reduction. The linewidth values for the MLL modes can be readily extracted from Figs. 6 and 11 because the FM-noise spectral density curves are already scaled for linewidth values to be read off. We average the three values at the lowest frequencies to estimate the linewidth and plot the linewidth values of the original MLL, phase noise reduced MLL, and phase noise

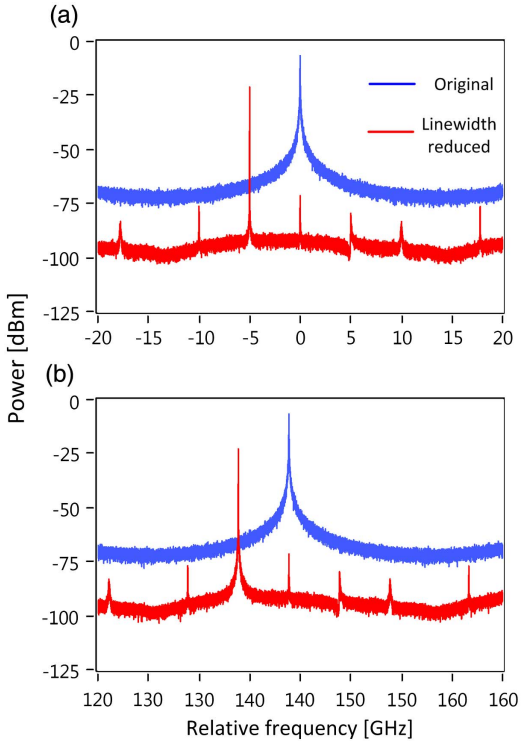

Fig. 10. Overlaid spectra of the original MLL and phase noise reduced MLL. Note the narrow line broadening of the reduced phase noise MLL compared to the original MLL. Plots of the 0th and 5th indexed modes are shown in (a) zoom at mode "0" and (b) zoom at mode "5," respectively.

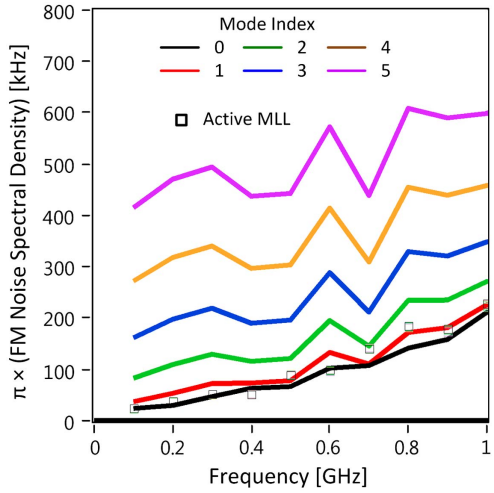

Fig. 11. Calculated FM-noise spectral density of the modes of the reduced phase noise MLL. Note how the value of the FM-noise spectral density asymptotically reduces to that of the values for the MLL with jitter-only in Fig. 6. If the MLL is actively mode-locked to a high-quality RF source with RF linewidth of 0 Hz such that there is no timing jitter, then the FM-noise spectral density for all modes are the same as shown by the black squares. The FM noise of the active MLL is the same as the mode that does not experience extra phase noise due to the timing jitter, i.e., the black line for the 0th indexed mode of the MLL with jitter.

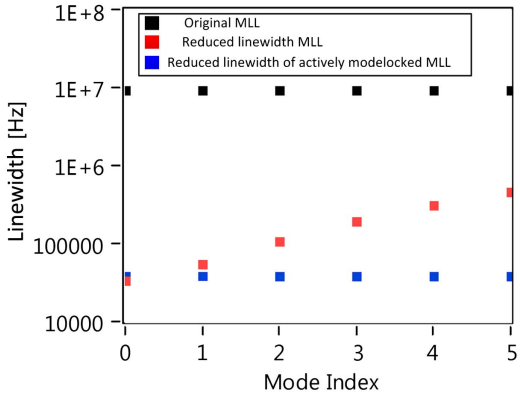

Fig. 12. Extracted linewidth of the modes for the original MLL (black), the reduced phase noise MLL (red) and reduced linewidth active MLL (blue). This figure shows explicitly the increase in line broadening due to the timing jitter. The result is similar to the experimental results shown in Figure 6 in [17].

reduced MLL in the active locking case in Fig. 12. We can clearly see the reduction in linewidth approaching that of the LO, which was 10 kHz. For the MLL with jitter, the linewidth increases with mode index number. A similar trend was presented in the experimental investigation to the linewidth reduction scheme [16,17]. The temporal jitter limits the ability of the phase noise reduction scheme to reduce the linewidth for all of the modes. Note that there is no visible increase in the linewidth for the active mode-locked MLL case given by the blue squares in Fig. 12. In order to effectively reduce the linewidth of all of the modes of an MLL, the MLL should be synchronized to a high-quality RF source that has an RF linewidth of just a few hertz.

4. PHASE NOISE RECOVERY OF QAM SYSTEMS

The phase noise reduction technique has enabled single-section semiconductor-based MLLs to transmit multi-Tbit/s transmission using quadrature phase shift keying [19,20]. In this section we investigate the potential of the phase noise reduction technique to transmit signals with 16- and 64-QAM and hence achieve spectral efficiencies approaching 6 bits/s/Hz/polarization. To do this we take the field of the phase noise reduced MLL and modulate with 16-QAM and 64-QAM signals using Nyquist pulse shaping techniques. We adopt a symbol rate of 27.278 GBaud, which is 500 MBaud less than the allowable maximum allowable baud rate imposed by the FSR of the MLL. This helps to eliminate cross talk from neighboring channels at the receiver. We are employing root-raised cosine pulse shaping for the optical signals and an equivalent matched filter in the receiver to select a single channel from the modulated MLL. The spectrum of the modulated MLL spectrum is shown in Fig. 13. The pulse shaping produces a flat spectrum without spectral spillage of the channels into the neighboring channel. The channel numbers for channel "0" and channel "5" are indicated, as well as a zoom in Fig. 13(b) to show the spectral guard band between the channels.

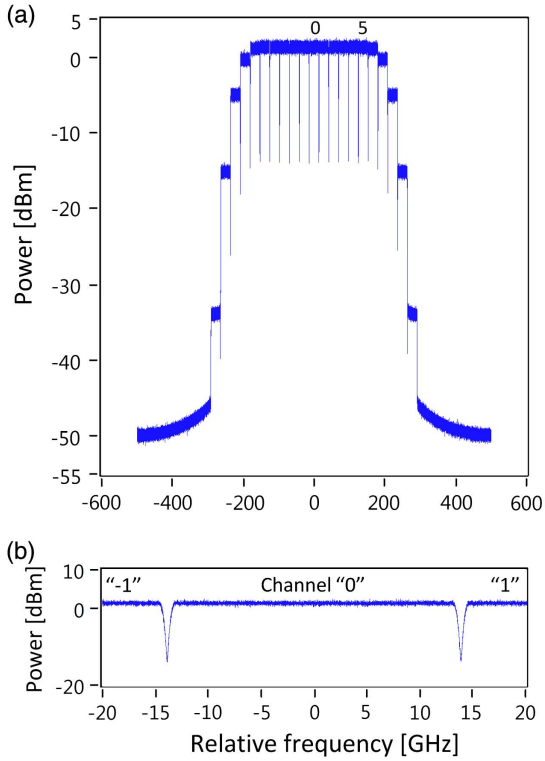

Fig. 13. Reduced phase noise MLL is modulated with data in 16-QAM format. Nyquist pulse shaping is used to obtain flat spectrum after data modulation. (a) NWDM spectrum shows the entire spectrum of the modulated MLL. (b) Zooms in on a portion to show the spectral guard band between the channels.

Note that when employing the phase noise reduction technique, we are dealing with the jitter of the MLL and the phase noise of the LO as the main phase noise sources in our communication system. We therefore plot the temporal jitter profile of the MLL implemented in the simulation in Fig. 14(a), and this is kept the same throughout this section to allow for a fair comparison with the entire set of results. The 1 ps jumps arise because the jitter is programmed to jump by ± 1 ps. We filter out the modulated field of the different modes with mode indices ranging from 0 to 5 using a root raised cosine matched filter. The symbols E_S are then retrieved and they now also contain the phase noise from the underlying MLL mode. The phase is principally the phase noise from the LO laser used in the phase noise reduction scheme and the MLL jitter. In the simulation we are able to completely eliminate the frequency offset between the carrier and an ideal local oscillator without phase noise in the receiver, and we therefore use a single-order decision-directed phase-locked loop to perform the carrier phase recovery process. The output of the QAM demodulator is given by comparing the phase-tracked received symbol with the entire constellation set and a hard decision (E_{HD}) that determines the most likely transmitted QAM signal. The tracked phase output from the decision-directed phase-locked loop is given by

$$\phi_{\mathrm{rec}}(k+1) = \phi_{\mathrm{rec}}(k) + \mu\,\mathrm{Im}\left\{\frac{\tilde{E}_S(k)E^*_{\mathrm{HD}}(k)}{|E_{\mathrm{HD}}(k)|^2}\right\}, \qquad (15)$$

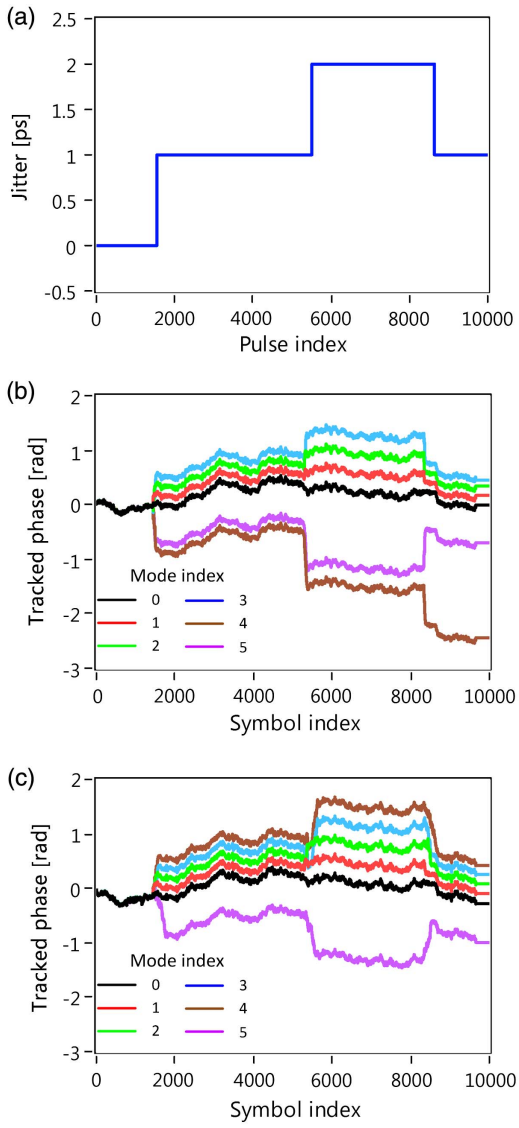

Fig. 14. (a) Jitter profile implemented on the MLL for all results in this figure. (b) Tracked phase for 16-QAM demodulation. Note the abrupt jumps in the tracked phase for the modes, and how for modes with indices 1 to 3, the carrier phase recovery tracks the jitter. Cycle slips occur for modes 4 and 5 due to the abrupt nature of the implemented timing jitter. (c) Carrier phase recovery after 64-QAM demodulation.

where ϕ_{rec} is the recovered phase of the optical carrier needed to keep track of the QAM symbols. The second term on the right-hand side estimates the phase difference between the phase-tracked received symbol $\tilde{E}_S(k) = E_S(k)\exp(-j\phi_{\text{rec}}(k))$ and the QAM demodulator output $E_{\text{HD}}(k)$; "Im" stands for the imaginary part. The loop update parameter μ defines the dynamics of the phase-locked loop and we set to 0.1 throughout this section.

The implementation in the simulations of the MLL jitter imposes abrupt phase changes, and one of the difficulties in performing carrier phase recovery on a signal with highly abrupt phase changes is that there is the possibility of a cycle slip in the carrier phase recovery process. Cycle slips occur because abrupt carrier phase changes greater than $\pi/4$ will cause incorrect symbol decisions to be made due to the $\pi/4$ rotational symmetry of the QAM constellations. Therefore, we need to limit the phase shift arising from the jitter to be less than $\pi/4$. We note that the expression for MLL-mode-dependent jitter-induced phase noise in Eq. (4), $\Delta\phi_m = 2\pi m\tau_j/T_P$; we ignore the optical linewidth, which has been significantly diminished by the linewidth reduction process. We need to impose the condition that $\Delta\phi_m$ be less than $\pi/4$, and therefore the condition that the phase shift for the mth mode index arising from the jitter must be $2\pi m\tau_j/T_P < \pi/4$. We are now in a position to give guidelines to set the sampling period in order to avoid artificial cycle slips during the carrier phase recovery of such systems. The implemented timing jitter τ_j equals t_s; therefore, we arrive at a condition relating the sampling time to the MLL repetition period and mode index number:

$$t_s < \frac{T_p}{8|m|}, \tag{16}$$

where t_s is the sampling time, T_P is the pulse repetition period, and m is the mode index number. For a given system application one can appropriately set the sampling time so that modes whose modal index magnitude does not exceed $|m|$ can be simulated without encountering an artificial cycle slip. Using the numbers in the simulation we expect the condition in Eq. (16) to break down for the $m = 5$ mode. The retrieved carrier phase from the output of the decision-directed phase-locked loop using Eq. (15) is plotted for modes with indices from 0 to 5 in Fig. 14(b) for 16-QAM and Fig. 14(c) for 64-QAM. Note the abrupt changes in retrieved carrier phase that correspond to the jitter events in Fig. 14(a). The magnitude of the abrupt phase changes increases with increasing mode index number. This is as expected since the abrupt phase changes are caused by the timing jitter. In between a jitter event, the phase noise arises primarily from the phase noise of the LO and is the same for all modes. The abrupt phase changes due to the numerical implementation of the timing jitter indeed can cause cycle slips as is evident for the case of 16-QAM for modes with indices 4 and 5. The cycle slips also occur at the same symbol indices for 64-QAM as they did for 16-QAM because the waveform of the phase noise reduced MLL was the same when simulating both modulation formats. For the case of 16-QAM in Fig. 14(b) the fourth mode endures a cycle slip at around the 1600th symbol; even though we would expect the fourth mode to be cycle slip free, the combination of the abrupt phase change due to the jitter and the symbol sequence conspires to induce a cycle slip and the condition imposed on the signal sampling period in Eq. (16) should be made more stringent to account for this.

To highlight the effectiveness of the phase noise reduced technique to enable the transmission of higher-order modulation format we plot the constellations of the received signals after the carrier recovery process; the results are shown in Fig. 15(a) for the retrieved 16-QAM constellation for the third mode and Fig. 15(b) for the third mode with 64-QAM modulation. Note that no symbol errors were detected for either of those plots. The data transmission simulation was repeated again, though on this occasion the MLL did not undergo phase

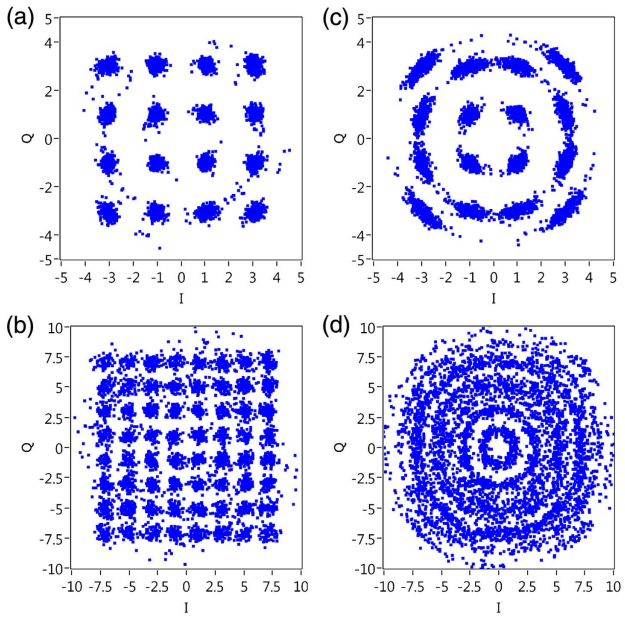

Fig. 15. Constellation diagrams after carrier phase recovery for (a), (c) 16-QAM and (b),(d) 64-QAM. In (a) and (b) the carrier was an MLL with reduced phase noise. In (c) and (d) the optical carrier was the original MLL with 10 MHz linewidth. The quality of the received constellations for signals carried by the reduced phase noise MLL are clearly superior to those constellations of signals carried by the original MLL with 10 MHz linewidth. All of the plots were taken for the $m = 3$. MLL mode.

noise reduction. The results are presented in Figs. 15(c) and 15(d). The large linewidth of 10 MHz causes the symbols to undergo larger angular spreading after the carrier phase recovery. The large angular spread of the constellation points will induce larger transmission penalties at the receiver. Note for 64-QAM in Fig. 15(d) that no discernible constellation points are visible indicating the inability for sources with linewidths of 10 MHz to be able to transmit 64-QAM signals and by using the phase noise reduction technique that sources with linewidths of 10 MHz could be used to transmit higher-order modulation formats, such as 64-QAM.

5. CONCLUSION AND DISCUSSION

We have shown how to create an easy to use MLL model that incorporates the timing jitter. The method ignores the mode-locking mechanism and is intended for an ease-of-use numerical source to study the effects of random-walk timing jitter from MLL-type pulse sources within system applications. The jitter can be referenced as a standard deviation of the differential pulse-to-pulse timing jitter or more conveniently as an RF linewidth. The use of a style of Schmitt trigger when implementing the accumulated jitter eliminates multiple bursts of jitter events that result in unrealistic high-frequency FM noise. We are ultimately limited by the signal sampling period, which needs to be chosen wisely depending on the system application. The pulse shape of the pulses can be chosen arbitrarily; the method for generating an MLL field with phase noise and jitter will work with any pulse shape including dispersed pulse shapes or those generated using a Hilbert transform so that the mode with the lowest linewidth would be at the edge of the spectrum as has been observed for single-section quantum dash MLLs. [10,18].

We use our MLL model to study the electro-optic phase noise reduction technique whereby the optical linewidth of the MLL modes are simultaneously reduced to that of a separate LO laser. Thus, the phase noise arising from the timing jitter is also present in the output of the phase noise reduction technique. The numerical study of the phase noise reduction technique here is in agreement with the experimental results that not all of the phase noise of the modes is cancelled due to the timing jitter. We verified this because the phase noises of the MLL including only timing jitter and that of the reduced phase noise MLL are similar. The difference between them is just the addition of the phase noise from the LO laser used in the reduction technique. Finally, we showed that the phase noise reduction technique could be used to enable MLLs to be able to transmit advanced modulation formats, such as 16- and 64-QAM modulation formats.

Funding. Science Foundation Ireland (SFI) (12/RC/2276); Irish Research Council (Ulysses).

REFERENCES

1. H. A. Haus, "Mode-locking of lasers," IEEE J. Sel. Top. Quantum Electron. **6**, 1173–1185 (2000).
2. F. X. Kärtner, *Few-Cycle Laser Pulse Generation and Its Applications* (Springer, 2004).
3. J. Javaloyes and S. Balle, "Mode-locking in semiconductor Fabry-Perot lasers," IEEE J. Quantum Electron. **46**, 1023–1030 (2010).
4. K. Yvind, D. Larsson, L. J. Christiansen, C. Angelo, L. K. Oxenløwe, J. Mørk, D. Birkedal, J. M. Hvam, and J. Hanberg, "Low-jitter and high-power 40-GHz all-active mode-locked lasers," IEEE Photon. Technol. Lett. **16**, 975–977 (2004).
5. R. Arkhipov, A. Pimenov, M. Radziunas, D. Rachinskii, A. G. Vladimirov, D. Arsenijevic, H. Schmeckebier, and D. Bimberg, "Hybrid mode locking in semiconductor lasers: simulations, analysis, and experiments," IEEE J. Sel. Top. Quantum Electron. **19**, 1100208 (2013).
6. J. Renaudier, G.-H. Duan, P. Landais, and P. Gallion, "Phase correlation and linewidth reduction of 40 GHz self-pulsation in distributed Bragg reflector semiconductor lasers," IEEE J. Quantum Electron. **43**, 147–156 (2007).
7. R. Rosales, K. Merghem, A. Martinez, A. Akrout, J.-P. Tourrenc, A. Accard, F. Lelarge, and A. Ramdane, "InAs/InP quantum-dot passively mode-locked lasers for 1.55-μm applications," IEEE J. Sel. Top. Quantum Electron. **17**, 1292–1301 (2011).
8. C. Calò, V. Vujicic, R. Watts, C. Browning, K. Merghem, V. Panapakkam, F. Lelarge, A. Martinez, B.-E. Benkelfat, A. Ramdane, and L. P. Barry, "Single-section quantum well mode-locked laser for 400 Gb/s SSB-OFDM transmission," Opt. Express **23**, 26442–26449 (2015).
9. M. Gioannini, P. Bardella, and I. Montrosset, "Time-domain traveling-wave analysis of the multimode dynamics of quantum dot Fabry-Perot lasers," IEEE J. Sel. Top. Quantum Electron. **21**, 698–708 (2015).
10. S. Latkowski, R. Maldonado-Basilio, K. Carney, J. Parra-Cetina, S. Philippe, and P. Landais, "Semiconductor optical amplifier-based heterodyning detection for resolving optical terahertz beat-tone signals from passively mode-locked semiconductor lasers," Appl. Phys. Lett. **97**, 081113 (2010).
11. Y. B. M'Sallem, Q. T. Le, L. Bramerie, Q.-T. Nguyen, E. Borgne, P. Besnard, A. Shen, F. Lelarge, S. LaRochelle, L. A. Rusch, and J.-C. Simon, "Quantum-dash mode-locked laser as a source for

56-Gb/s DQPSK modulation in WDM multicast applications," IEEE Photon. Technol. Lett. **23**, 453–455 (2011).
12. J. Müller, J. Hauck, B. Shen, S. Romero-García, E. Islamova, S. S. Azadeh, S. Joshi, N. Chimot, A. Moscoso-Mártir, F. Merget, F. Lelarge, and J. Witzens, "Silicon photonics WDM transmitter with single section semiconductor mode-locked laser," Adv. Opt. Technol. **4**, 119–145 (2015).
13. V. Vujicic, C. Calò, R. Watts, F. Lelarge, C. Browning, K. Merghem, A. Martinez, A. Ramdane, and L. P. Barry, "Quantum dash mode-locked lasers for data centre applications," IEEE J. Sel. Top. Quantum Electron. **21**, 53–60 (2015).
14. J. Pfeifle, I. Shkarban, S. Wolf, J. N. Kemal, C. Weimann, W. Hartmann, N. Chimot, S. Joshi, K. Merghem, A. Martinez, M. Weber, A. Ramdane, F. Lelarge, W. Freude, and C. Koos, "Coherent terabit communications using a quantum-dash mode-locked laser and self-homodyne detection," in *Proceedings of the Optical Fiber Communication Conference*, Los Angeles, California, USA (2015), paper W2A.19.
15. T. N. Huynh, R. Watts, V. Vujicic, M. D. Gutierrez Pascual, C. Calo, K. Merghem, V. Panapakkam, F. Lelarge, A. Martinez, B.-E. Benkelfat, A. Ramdane, and L. P. Barry, "200-Gb/s baudrate-pilot-aided QPSK/direct detection with single-section quantum-well mode-locked laser," IEEE Photon. J. **8**, 7903107 (2016).
16. R. Watts, S. G. Murdoch, and L. P. Barry, "Spectral linewidth reduction of single-mode and mode-locked lasers using a feed-forward heterodyne detection scheme, in *Proceedings of the Conference on Lasers and Electro-Optics (CLEO)*, San Jose, California, USA (2014), paper STh3O.8.
17. R. T. Watts, S. G. Murdoch, and L. P. Barry, "Phase noise reduction of an optical frequency comb using a feed-forward heterodyne detection scheme," IEEE Photon. J. **8**, 7900707 (2016).
18. M. O. Sahni, S. Trebaol, L. Bramerie, M. Joindot, S. P. Ó Dúill, S. G. Murdoch, L. P. Barry, and P. Besnard, "Frequency noise reduction performance of a feed-forward heterodyne technique: application to an actively mode-locked laser diode," Opt. Lett. **42**, 4000–4003 (2017).
19. J. Pfeifle, R. Watts, I. Shkarban, S. Wolf, V. Vujicic, P. Landais, N. Chimot, S. Joshi, K. Merghem, C. Calò, M. Weber, A. Ramdane, F. Lelarge, L. Barry, W. Freude, and C. Koos, "Simultaneous phase noise reduction of 30 comb lines from a quantum-dash mode-locked laser diode enabling coherent Tbit/s data transmission," in *Proceedings of the Optical Fiber Communication Conference* (2015), paper Tu3I.5.
20. W. Freude, J. Pfeifle, R. Watts, I. Shkarban, S. Wolf, V. Vujicic, P. Landais, N. Chimot, S. Joshi, K. Merghem, C. Calò, M. Weber, A. Ramdane, F. Lelarge, L. Barry, and C. Koos, "Phase-noise compensated carriers from an optical frequency comb allowing terabit transmission," in *Proceedings of the 17th International Conference on Transparent Optical Networks (ICTON)*, Budapest, Hungary, July (2015), paper Tu.B5.1.
21. F. Aflatouni and H. Hashemi, "Wideband tunable laser phase noise reduction using single sideband modulation in an electro-optical feed-forward scheme," Opt. Lett. **37**, 196–198 (2012).
22. L. Drzewietzki, S. Breuer, and W. Elsaßer, "Timing jitter reduction of passively mode-locked semiconductor lasers by self- and external-injection: numerical description and experiments," Opt. Express **21**, 16142–16161 (2013).
23. S. P. O'Duill, R. Zhou, P. Anandrajah, and L. P. Barry, "Analytical approach to assess the impact of pulse-to-pulse phase coherence of optical frequency combs," IEEE J. Quantum Electron. **51**, 1200208 (2015).
24. R. Maldonado-Basilio, J. Parra-Cetina, S. Latkowski, and P. Landais, "Timing-jitter, optical, and mode-beating linewidths analysis on subpicosecond optical pulses generated by a quantum-dash passively mode-locked semiconductor laser," Opt. Lett. **35**, 1184–1186 (2010).
25. T. Habruseva, S. O'Donoghue, N. Rebrova, F. Kéfélian, S. P. Hegarty, and G. Huyet, "Optical linewidth of a passively mode-locked semiconductor laser," Opt. Express **34**, 3307–3309 (2009).
26. Y. Takushima, H. Sotobayashi, M. E. Grein, E. P. Ippen, and H. A. Haus, "Linewidth of mode combs of passively and actively mode-locked semiconductor laser diodes," Proc. SPIE **5595**, 213–227 (2004).
27. R. W. Hamming, *Digital Filters*, 3rd ed. (Prentice-Hall, 1998).
28. J. Mulet and J. Mørk, "Analysis of timing jitter in external-cavity mode-locked semiconductor lasers," IEEE J. Quantum Electron. **42**, 249–256 (2006).
29. D. Marcuse, "Computer simulation of FSK laser spectra and of FSK-to-ASK conversion," J. Lightwave Technol. **8**, 1110–1122 (1990).
30. F. Kéfélian, S. O'Donoghue, M. T. Todaro, J. G. McInerney, and G. Huyet, "RF linewidth in monolithic passively mode-locked semiconductor laser," IEEE Photon. Technol. Lett. **20**, 1405–1407 (2008).
31. S. P. Ó Dúill, A. P. Anthur, T. N. Huynh, S. T. Naimi, L. Nguyen, D. Venkitesh, and L. P. Barry, "Numerical generation of laser-resonance phase noise for optical communication simulators," Appl. Opt. **54**, 3398–3406 (2015).
32. S. P. O'Duill, S. T. Naimi, A. P. Anthur, T. N. Huynh, D. Venkitesh, and L. P. Barry, "Simulations of an OSNR-limited all-optical wavelength conversion scheme," IEEE Photon. Technol. Lett. **25**, 2311–2314 (2013).
33. S. T. Naimi, S. P. Ó Dúill, and L. P. Barry, "All optical wavelength conversion of Nyquist-WDM superchannels using FWM in SOAs," J. Lightwave Technol. **33**, 3959–3967 (2015).
34. K. Kikuchi, "Characterization of semiconductor-laser phase noise and estimation of bit-error rate performance with low-speed offline digital coherent receivers," Opt. Express **20**, 5291–5302 (2012).
35. T. Kawanishi, T. Sakamoto, T. Miyazaki, M. Izutsu, T. Fujita, S. Mori, K. Higuma, and J. Ichikawa, "High-speed optical DQPSK and FSK modulation using integrated Mach-Zehnder interferometers," Opt. Express **14**, 4469–4478 (2006).
36. C. Henry, "Theory of the phase noise and power spectrum of a single mode injection laser," IEEE J. Quantum Electron. **19**, 1391–1397 (1983).